Journal of Alloys and Compounds 883 (2021) 160865

Contents lists available at ScienceDirect

Journal of Alloys and Compounds

journal homepage: www.elsevier.com/locate/jalcom

Superelastic damping at nanoscale in ternary and quaternary Cu-based shape memory alloys

J.F. Gómez-Cortés[a,*], V. Fuster[a,b], M. Pérez-Cerrato[a], P. Lorenzo[a], I. Ruiz-Larrea[a], T. Breczewski[a], M.L. Nó[a], J.M. San Juan[a]

[a] Dpt. de Física, Facultad de Ciencia y Tecnología, Universidad del País Vasco UPV/EHU, Apdo. 644, 48080 Bilbao, Spain
[b] Instituto de Física Rosario, Consejo Nacional de Investigaciones Científicas y Técnicas (CONICET)-Universidad Nacional de Rosario, 2000 Rosario, Argentina

ARTICLE INFO

Article history:
Received 17 May 2021
Accepted 16 June 2021
Available online 18 June 2021

Keywords:
Shape Memory Alloys
Cu-based alloys
Superelasticity
Mechanical damping
Size effect
Internal friction
Nanoindentation

ABSTRACT

Superelasticity is a characteristic thermomechanical property in shape memory alloys (SMA), which is due to a reversible stress-induced martensitic transformation. Nano-compression experiments made possible the study of this property in Cu–Al–Ni SMA micropillars, showing an outstanding ultra-high mechanical damping capacity reproducible for thousands of cycles and reliable over the years. This scenario motivated the present work, where a comparative study of the damping capacity on four copper-based SMA: Cu–Al–Ni, Cu–Al–Be, Cu–Al–Ni–Be and Cu–Al–Ni–Ga is approached. For this purpose, [001] oriented single-crystal micropillars of comparable dimensions (around 1 μm in diameter) were milled by focused ion beam technique. All micropillars were cycled up to two hundred superelastic cycles, exhibiting a remarkable reproducibility. The damping capacity was evaluated through the dimensionless loss factor η, calculated for each superelastic cycle, representing the dissipated energy per cycle and unit of volume. The calculated loss factor was averaged between three micro-pillars of each alloy, obtaining the following results: Cu–Al–Ni η = 0.20 ± 0.01; Cu–Al–Be η = 0.100 ± 0.006; Cu–Al–Ni–Be η = 0.072 ± 0.004 and Cu–Al–Ni–Ga η = 0.042 ± 0.002. These four alloys exhibit an intrinsic superelastic damping capacity and offer a wide loss factor band, which constitutes a reference for engineering, since this kind of micro/nano structures can potentially be integrated not only as sensors and actuators but also as dampers in the design of MEMS to improve their reliability. In addition, the study of the dependence of the superelastic loss factor on the diameter of the pillar was approached in the Cu–Al–Ni–Ga alloy, and here we demonstrate that there is a size effect on damping at the nanoscale.

1. Introduction

Mechanical damping is the energy attenuation of a mechanical force disturbance. This attenuation capacity is a mechanical property that has attracted the interest of many industrial sectors, for a variety of applications, to solve problems associated with acoustic noise pollution, structural vibration in diverse working conditions such as in tool machining, electronic equipment and aerospace aircraft structures, as well as for seismic waves mitigation in buildings, just to give some examples [1–3]. To approach the study and characterization of damping, some phenomenological aspects and mathematical tools for its analysis have been developed [4–9], offering the required background in this field. Thus, the development of high-damping materials (HDM) offers a potential solution in many practical situations where passive damping is required [10–12] or even to optimize the combination of active and passive damping [3].

Among the different families of HDM, shape memory alloys (SMA) constitute one of the most important materials because of their intrinsic high damping associated with the mobility of the interfaces [13–16]. Indeed, SMA undergo a thermo-elastic martensitic phase transformation (MT) based on a reversible crystal lattice shearing mechanism that drives the transition from a high-temperature phase, called austenite, to a low-temperature phase defined as martensite [17–19]. Depending on the trigger stimulus, the MT can give place to two outstanding thermo-mechanical effects, the shape memory effect when it is thermally-induced, and the superelastic effect when it is stress-induced (SIMT) [17–19]. Thus, at a given constant temperature, SMA exhibit a high intrinsic damping capacity associated with the displacement of the martensite/martensite interfaces in the martensitic state or/and to the displacement

* Corresponding author.
E-mail address: josefernando.gomez@ehu.es (J.F. Gómez-Cortés).

https://doi.org/10.1016/j.jallcom.2021.160865
0925-8388/

of martensite/austenite interfaces during the superelastic effect by SIMT, giving place to numerous damping applications from noise cancellation to civil engineering [20–23].

The superelastic effect is a non-linear mechanical behavior characterized by a hysteretic loop on the stress-strain field during the SIMT cycle [18,19], implying the occurrence of an energy dissipation process and being responsible for a high mechanical damping capacity, which is the subject matter of the present work. The hysteresis loop area encloses the energy invested, for nucleation and progress of the austenite/martensite interfaces, which mediates through the forward and reverse transformation. Then, the dissipated energy is directly proportional to the stress hysteresis, $\Delta\sigma_{hys}$, defined as the difference between the critical stress needed to start the nucleation of the martensite phase, σ_{Ms}, during the forward transformation, and the stress at which the austenite parent phase is recovered, σ_{Af}, when withdrawing the load during the reverse transformation. Therefore, $\Delta\sigma_{hys}$ is a factor that defines the superelastic effect in SMA, and the study of its appearance, line shape and magnitude has fundamental and technological implications.

In this context, Ni–Ti based SMA have been extensively studied, see [24] for a review, and dominates the international market because of their many successful applications [19,25]. Nevertheless, in the last decades Cu-based SMA have attracted a renewed interest, in particular the Cu–Al–Ni family, because of their remarkable thermo-mechanical properties. Indeed, since the pioneering works of Otsuka et al. [26–29], many works have been performed on this family of alloys, studying its anisotropic behavior [30–33], the influence of composition, thermal treatments and precipitation of the stable phases [34–40] on the martensitic transformation, as well as their thermo-mechanical behavior [30,32,41–47]. Other Cu-based SMA, as for instance the system of Cu–Al–Be [48–55], are being extensively studied, but it is not our goal to do a general review on all Cu-Based SMA in the present paper, which will be focused mainly in Cu–Al–Ni and Cu–Al–Be SMA.

The advent of the miniaturization trend motivated the study of SMA at small scale to expand engineering alternatives needed to design a new generation of smart micro electro-mechanical systems (MEMS) [56–58]. In this regard, during the last years, nano-compression experiments have been used to study 3D micro and sub-micro structures of several SMA. The idea was to use nanoindentation techniques [59,60] to approach the behavior of SMA at micro and nanoscale and elucidate whether their thermo mechanical properties exhibit size effects similar to the ones reported in plasticity [61–63]. These experiments allow measuring, at the μN range of force and the nm length scale, the force-displacement response during a loading-unloading cycle and were used to study the superelastic effect in SMA. Whereas Ni-Ti micropillars exhibited a loss of superelasticity due to plastic deformation [64], a perfect and reproducible superelastic cycle was measured in Cu–Al–Ni micropillars [65], as well a good shape memory effect at the same scale [66]. In addition, an outstanding ultra-high damping coefficient was reported at nanoscale in Cu–Al–Ni nano pillars [67] and attributed to a size effect on superelasticity. Nevertheless, no size effects were observed in Ni-Ti [68] and Greer & De Hosson [69] published a review in which any trend concerning size effects on SMA could be concluded yet. However, a size effect on the selection rules of martensites at small scale was reported by in-situ superelastic tests performed at the transmission electron microscope [70], and a general view on the size effects in SMA was discussed in ref. [71]. Since then, many works have been carried out in micro pillars of different SMA, and even in shape memory ceramics [72–79], but not clear evidence was offered about size effects until the recent works on Cu–Al–Ni [80] and Cu–Al–Be [81], which reported an outstanding size effect on the critical stress for superelasticity below one micrometer of pillar diameter, and offered an explanation whose model fit very well the experimental results. In addition, Cu–Al–Ni SMA stand out for a good long-term cycling behavior at the nanoscale [82,83] and a robust superelastic behavior, with an ultra-high damping capacity, reproducible for thousands of cycles and with high reliability over the years [83]. These results are promising for the SMA integration to MEMS designs, not only as active elements for actuation and sensing, but also for damping purposes. Indeed, new trends of vacuum packaging, to improve MEMS sensitivity [84,85], suppress the air squeeze damping, exacerbating the mechanical vibration problem, which constitutes one of the most critical issues for MEMS reliability [86]. In this scenario, the use of SMA for damping at micro and nanoscale open a new way to improve the MEMS reliability.

Looking forward in this direction, the present work aims to measure the superelastic behavior at the nanoscale, and the associated damping capacity, in four Cu-based SMA, two ternary alloys Cu–Al–Ni and Cu–Al–Be, as well as two quaternary alloys Cu–Al–Ni–Be and Cu–Al–Ni–Ga, in order to present a comparative analysis of their mechanical damping capacity at small scale. For this purpose, several micropillars of similar dimensions (about 1 μm diameter) were tested in nano-compression over two hundred superelastic cycles, calculating the loss factor η for each cycle. The loss factor was measured in several micropillars of the same alloy, obtaining a remarkable reproducibility, which will be carefully discussed, allowing consider the average value of damping as characteristic of the alloy system. The results are analyzed and compared for the different mechanical damping behavior observed in each alloy. Finally, we present experimental evidence that shows a size effect on the mechanical damping capacity at small scale in Cu–Al–Ni–Ga SMA.

2. Materials and methods

2.1. Samples and pillar machining

Four Cu-based SMA are studied in this work, two ternary alloys from Cu–Al–Ni and Cu–Al–Be systems, and two quaternary alloys Cu–Al–Ni–Be and Cu–Al–Ni–Ga, whose compositions are given in Table 1, and hereinafter referred as CAN, CAB, CANB and CANG respectively. In all cases, the samples of the studied alloys were cut from [001] oriented single crystals grown by the Bridgman method. The chemical compositions of the alloys were measured by induction coupled plasma (ICP) emission spectroscopy technique (Q-ICP-MS Thermo X Series-II). These alloys were selected to be in austenite phase at room temperature [35,48,87], in order to study the SIMT during nano-compression tests at room temperature conditions. The transformation temperatures were measured using a differential scanning calorimetry (DSC) equipment (Thermal Analysis Q-2000) and the martensite start (M_s) and the austenite finish (A_f) temperatures are also indicated in Table 1. Slices of about three millimeters thick of each sample were annealed at 1173 K in argon atmosphere and quenched in ice water, except the CAB sample, which was annealed at 1023 K and quenched in boiling water [54]. Finally, the samples were metallographically prepared on the (001)

Table 1
Chemical composition and martensitic transformation temperatures (Ms and Af) of the four Cu-based shape memory alloys in which [001] oriented single-crystal micropillars were milled to approach the present study.

Sample	Alloy Composition	Transformation temp.	
Code	(%wt.)	M_s (ºC)	A_f (ºC)
CAN	$Cu_{82.1}$–$Al_{13.9}$–$Ni_{4.0}$	-30	0
CAB	$Cu_{87.3}$–$Al_{12.2}$–$Be_{0.5}$	-26	-10
CANB	$Cu_{83.0}$–$Al_{12.5}$–$Ni_{4.2}$-$Be_{0.3}$	-82	-63
CANG	$Cu_{80.2}$–$Al_{14.1}$–$Ni_{4.6}$-$Ga_{1.1}$	-98	-65

oriented surface by polishing until 1 μm with diamond and finishing with 0.05 μm with alumina.

Micropillars of about 1 μm in diameter, and aspect ratio (diameter/height) between 1/3 and 1/5, as recommended for micro-compression tests [88], were milled by the focused ion beam (FIB) technique using a FEI Helios 650 Nanolab. The FIB milling was performed at 30 kV with a sequence of decreasing currents in several annular milling steps, as was described in previous works [65–67]. In total, three micropillars per sample were studied, with diameters ranging from 860 nm to 1100 nm, measured as described in Ref. [80]; this diameter range was selected to avoid the size effect on the critical stress observed in these families of alloys [80,81]. Finally, a series of pillars with different diameters, ranging from 2 μm down to 250 nm, was specifically milled on the CANG alloy, to approach the study of the potential existence of a size effect on damping.

2.2. Nano-compression tests and analysis

Nano-compression experiments were performed by instrumented nanoindentation using a Hysitron Triboindenter TI-950, equipped with an sphero-conical diamond indenter of 2 μm radius, according to the procedure described in more detail in previous works [65,82,83]. With the aid of a scanning probe mode image, the apex of the indenter was carefully positioned on the top of micropillars to run multiple-cycle tests (typically ten cycles) in load control mode, with a constant loading-unloading rate ranging from 150 to 250 μN/s. The load control mode was chosen because the alternative displacement control mode requires a continuous electronic feedback, which may introduce experimental artifacts in the case of very fast displacements. Maximum loads in the range of 130–500 μN were used, depending on the pillar diameter. The load function was repeatedly executed to accumulate up to 200 superelastic cycles in each studied micropillar. Nano-compression tests were performed at room temperature, 298 ± 1 K, measured with a sensor incorporated on the granite bridge of the TI-950; thermal drift was analyzed and automatically corrected by the TriboScan software.

The graph in Fig. 1 depicts a typical superelastic cycle obtained from a nano-compression experiment, in this particular case, performed on a 930 nm diameter micropillar, corresponding to CAN-P1 in Fig. 2(a). The loading curve initially shows the linear elastic regime of the austenite phase up to 100 μN, where it deviates from the linear behavior, and close to 120 μN is discontinued by a sudden and

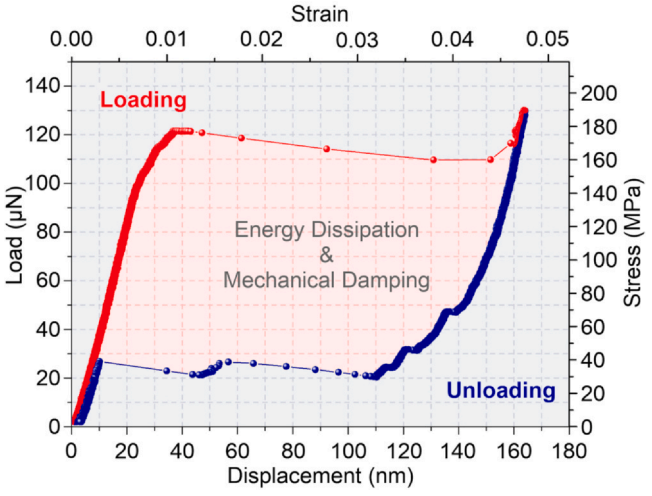

Fig. 1. Superelastic response in a load-displacement and stress-strain double-axis graph obtained during a nano-compression cycle. Loading curve involves the maximum applied energy (area under the load curve). Unloading curve draws a close hysteresis cycle whose internal area is the dissipated energy (loop area). The definition of the loss factor η relates these two areas in Eq. (1).

speedy displacement, about a hundred nanometers, at a nearly constant force. This plateau is a consequence of the SIMT triggered when the elastically stressed austenite reaches the load corresponding to the critical stress σ_{Ms} for the SIMT. From this point, the martensite domains grow fast in the load direction, allowing accommodate a significant displacement above 100 nm corresponding to almost 4% strain. The transformation plateau shows a slight decrease of the load due to the collapse of the pillar, since the SIMT occurs faster than the speed of the apex displacement determined by the loading rate, promoting the loss of contact and decreasing the load measured by the indenter. The unloading curve shows that the total displacement is fully recovered during the reverse MT drawing a hysteresis loop, whose area represents the energy dissipated during a superelastic transformation cycle, and the mechanical damping capacity linked to this behavior was studied in terms of the loss factor η, which for a compression test is mathematically defined as [6,67]:

$$\eta = \frac{\Delta W}{\pi \cdot W_{Max}} \tag{1}$$

Indeed, the loss factor η is a dimensionless index that relates the dissipated energy ΔW (hysteresis area) with the maximum applied energy W_{Max} (loading curve area) per cycle, and can reach a maximum value of $0.318 = 1/\pi$, in the case of a hypothetical full mechanical damping. Fig. 1 also shows the corresponding stress and strain axis in order that the reader could make an easier comparison with the macroscopic tests from the literature. However, it is worthy to note that, because of its definition, the loss factor η can be measured directly from the load-displacement curves, avoiding the potential errors coming from transforming load to stress and displacement to strain; this is the procedure used in the present work to evaluate the loss factor.

3. Results and discussion

3.1. Damping in ternary and quaternary alloys

Fig. 2(a) and (c) shows two scanning electron micrographs as representative examples of the micropillars, studied for the two ternary alloys of Cu–Al–Ni and Cu–Al–Be, specifically CAN-P1 and CAB-P3 with diameters of 930 nm and 920 nm respectively, together with their respective superelastic response, Fig. 2(b) and (d), tested at the nanoindenter. These curves correspond to the superelastic cycle number 30 (C30) of said micropillars. The cycles are plotted in a double-axis frame, the load-displacement scale as was experimentally measured, and the stress-strain scale obtained from the micropillars dimensions, measured as described in [80]. As can be seen, a fully closed superelastic cycle response was observed in both cases, and this behavior endured during the two hundred cycles performed on each one of the micropillars under study, as will be exposed later. The critical stress is similar in both alloys because of the proximity of their transformation temperatures, as shown in Table 1. The main qualitative difference is that whereas CAN-P1 pillar, in Fig. 2(b), shows only one plateau stage of superelastic deformation during loading, CAB-P3 pillar, in Fig. 2(d), exhibits a superelastic plateau followed by a second stage associated with the nucleation of a differently oriented set of martensite variants, activated by the local stresses, as was recently discussed in Ref. [83]. The loss factor η, calculated through Eq. (1), is indicated in each graph.

Following the same format of Fig. 2, Fig. 3(a) and (c) present two micrographs of the micropillars milled in the quaternary alloys of Cu–Al–Ni–Be (CAN) and Cu–Al–Ni–Ga, (CANG); specifically the micropillars CANB-P1, Fig. 3(a), and CANG-P1, Fig. 3(c), with diameters of 1020 nm and 1050 nm, respectively. The corresponding superelastic cycles are shown in Fig. 3(b) and (d) and in both pillars a higher critical stress than the one measured in the pillars of Fig. 2 is

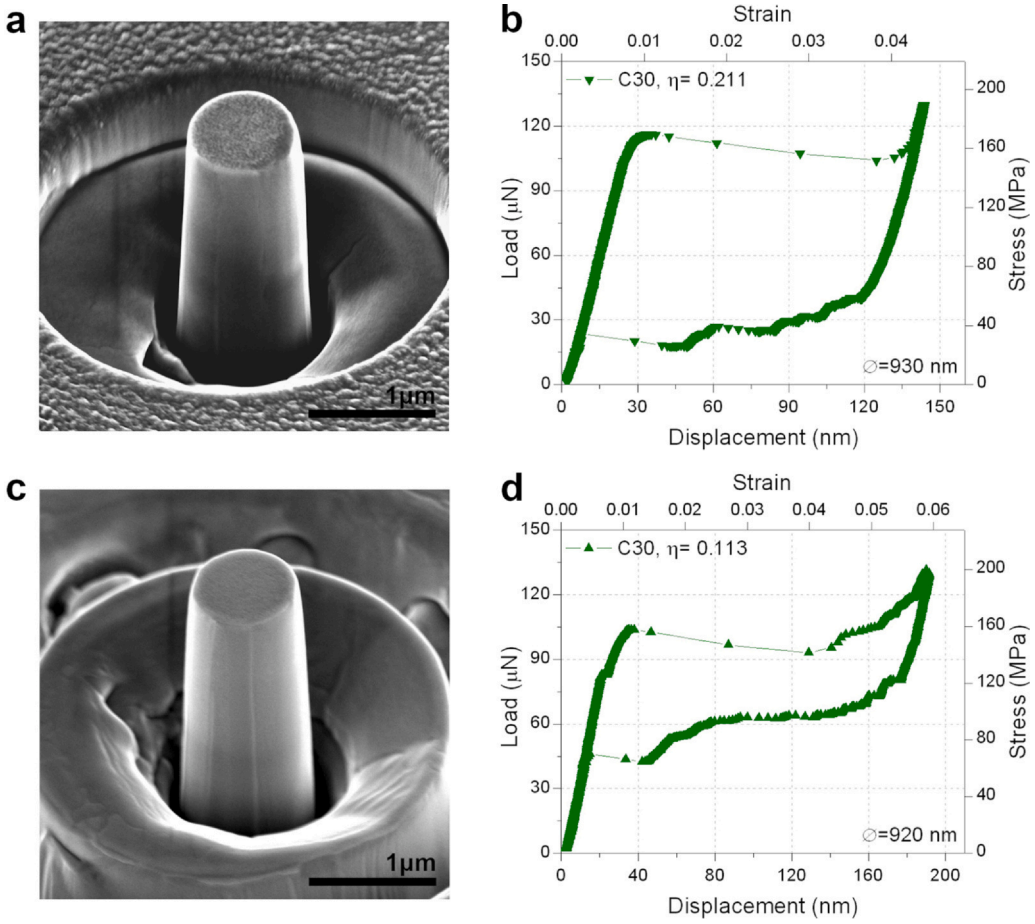

Fig. 2. Scanning electron microscopy images of two [001] oriented pillars milled on the samples (a) Cu–Al–Ni (CAN-P1) and (c) Cu–Al–Be (CAB-P3). (b), (d) Load-displacement and stress–strain double-axis curves obtained during the 30th superelastic nano-compression cycle; the curves (b) and (d) correspond to the pillar on its left.

observed, as could be expected from the lower transformation temperatures, see Table 1. Besides, a higher critical load is also expected due to the slightly larger diameters than the pillars presented in Fig. 2. The superelastic cycles look rather similar in these two quaternary alloys, although they exhibit a shorter first stage plateau than in the ternary alloys. The hysteresis loop evidences a different level of superelastic damping between the quaternary and the ternary alloys.

An alternative method to describe the damping capacity of the SMA during superelastic tests is to measure the mechanical hysteresis $\Delta\sigma_{hys} = \sigma_{Ms}-\sigma_{Af}$ as the critical stress difference between the loading and the unloading curves. This hysteresis is currently measured at macroscopic scale when the damping coefficient η cannot be easily measured. Obviously a correlation between the loss factor and the mechanical hysteresis can be established [7]. In Fig. 2 and Fig. 3, the mechanical hysteresis was measured through a straight line from the beginning of the superelastic plateau till the interception down at the end of the recovery in the unloading curve. Following this method, the mechanical hysteresis measured in each one of the alloys was: Fig. 2(b) 140 MPa in CAN; Fig. 2(d) 94 MPa in CAB; Fig. 3(b) 88 MPa in CANB; Fig. 3(d) 61 MPa in CANG. As expected, the higher the mechanical hysteresis, the greater the loss factor and hence the mechanical damping capacity. However, it should be remarked that the loss factor η can be precisely determined from the load-displacement curves, whereas the mechanical hysteresis can only be calculated from the stress-strain curves; the values of the mechanical hysteresis evaluated from the load-displacement curves would be dependent on the size of the pillar, making the comparison between different pillars and alloys impossible. Then, in what follows, the loss factor η will be the parameter used to characterize the damping behavior.

Taking the highest loss factor η obtained in the two sets of alloys in Fig. 2 and Fig. 3 as a reference, the calculated values are compared in what follows. The damping capacity of the two ternary alloys, CAN and CAB (Fig. 2), shows a notable difference of 46%, with $\eta = 0.211$ in the CAN-P1 micropillar and $\eta = 0.113$ in the CAB-P3 micropillar. For the two quaternary alloys, CANB and CANG (Fig. 3), this difference is 34%, with $\eta = 0.067$ in the CANB-P1 micropillar and $\eta = 0.044$ in the CANG-P1 micropillar. The difference between the damping capacity of ternary and quaternary alloys is even more remarkable. The loss factor exhibits a maximum difference of 79% when comparing the values regarding CAN-P1 and CANG-P1 micropillars.

From these results, the studied alloys can be preliminary ordered based on the damping capacity, from highest to lowest, as follows: CAN $\eta = 0.211$; CAB $\eta = 0.113$; CANB $\eta = 0.067$; CANG $\eta = 0.044$. However, these values should be taken with caution because they have been obtained from a particular superelastic cycle.

3.2. Nano-compression damping reproducibility

As commented before, in the present work we studied three micropillars per sample, and all of them were cycled 200 times. Fig. 4 exhibits the particular case of the three micropillars (P1, P2, P3) of the samples CAB (Fig. 4(a), (b), (c)) and CANG (Fig. 4(d), (e), (f)) to illustrate the typical superelastic observed behavior; the micropillar diameter is indicated in each case. In this Fig. 4, each graph depicts the superelastic cycles number 50, 100 and 200 of the mentioned micropillars and the loss factor η of each cycle is also

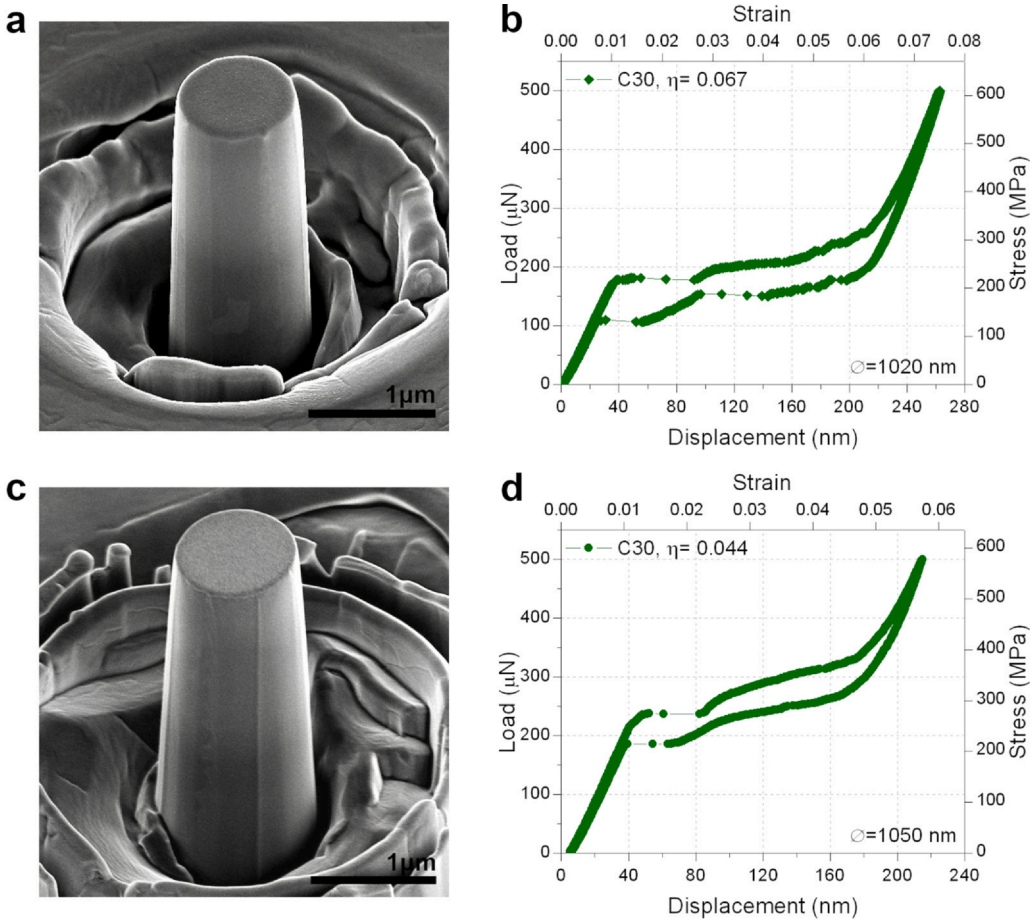

Fig. 3. Scanning electron microscopy images of two [001] oriented pillars milled on the samples (a) Cu–Al–Ni–Be (CANB-P1) and (c) Cu–Al–Ni–Ga (CANG-P1). (b), (d) Load-displacement and stress-strain double-axis curves obtained during the 30th superelastic nano-compression cycle; the curves (b) and (d) correspond to the pillar on its left.

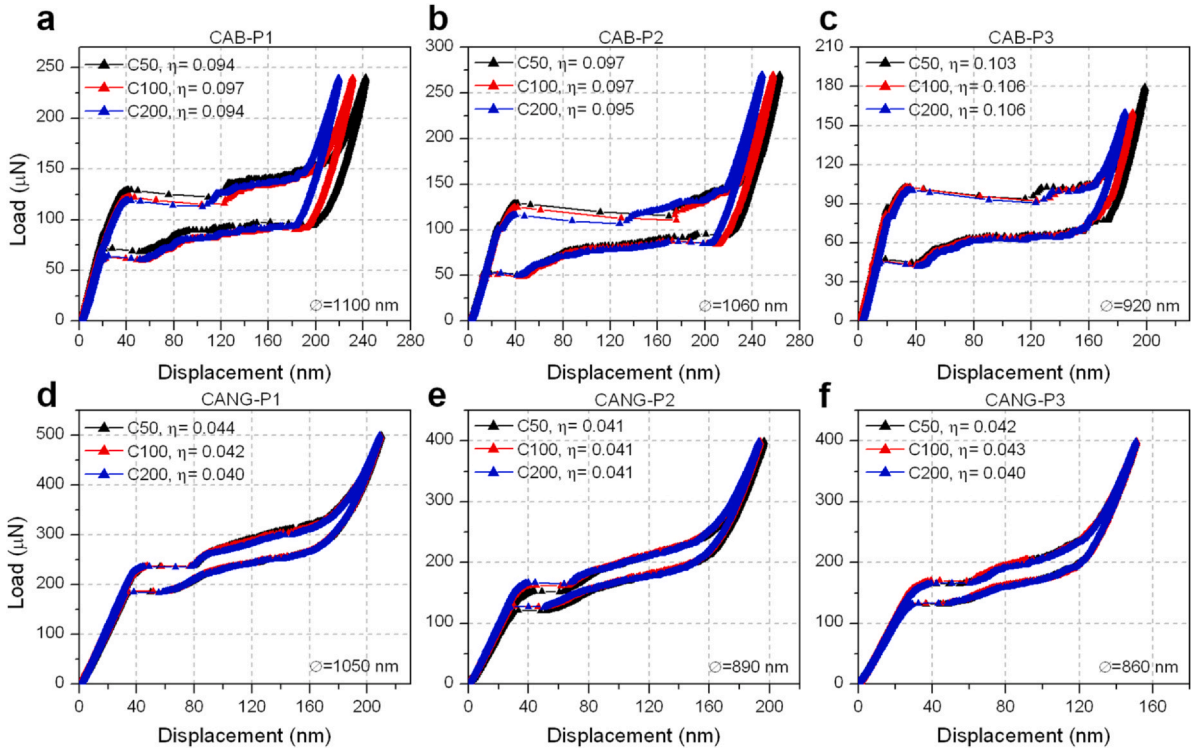

Fig. 4. Load-displacement curves measured in the 50, 100 and 200 superelastic cycles on the three pillars (P1 to P3) milled in each alloy: (a)-(c) for the Cu–Al–Be, and (d)-(f) for the Cu–Al–Ni–Ga. The loss factor η for each superelastic curve and the diameter (Ø) of the corresponding pillar are also indicated.

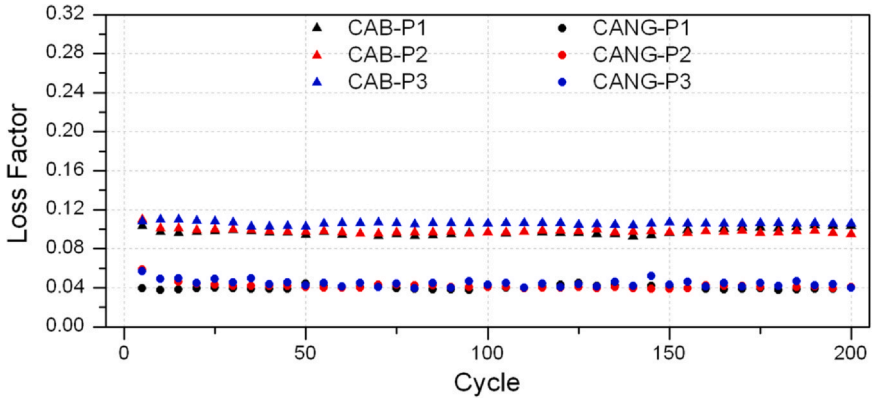

Fig. 5. Loss factor measured as a function of cycling for two sets of three different pillars (P1 to P3) of each alloy. One set of pillars milled in the CAB alloy (upward triangles), and the other set of pillars milled in the CANG alloy (dots).

included. During cycling, the superelastic behavior shows an evolution that stabilizes quickly in the first thirty cycles, and for each micropillar exhibits a remarkable reproducibility along the two hundred cycles tested, as can be seen in Fig. 4 where the cycles 50, 100 and 200 are superimposed, the loop line-shapes barely show any difference. In terms of the loss factor η, the reproducibility was measured with a deviation smaller than 3% for each micropillar. This behavior agrees with previous works where long-term superelastic cycling was studied in square-section micropillars in the CAN sample [82,83], and now it is also confirmed in micropillars of the CAB, CANB and CANG samples. It is worthy to note the exceptional reproducibility and stability along cycling of the superelastic behavior in the quaternary CANG alloy. To illustrate the damping behavior along cycling, Fig. 5 shows the loss factor as a function of the number of cycles for the three micropillars of the CAB and CANG samples. In this Fig. 5, it can be clearly seen that the three different micropillars of each sample present a narrow distribution of the loss factor, forming two levels, one for the CAB sample (upward triangles) and the other for the CANG sample (dots). The standard deviation of the averaged loss factor between micropillars, even with different diameter, does not exceed 5% in the case of more significant variation, which was for the micropillars of CANB sample. Taking into account this small deviation of the loss factor, its average value for the different pillars could represent the characteristic mechanical damping associated with the corresponding alloy. Thus, the average loss factor profile along cycling measured for each alloy is depicted in Fig. 6. In this graph, four profiles of mechanical damping can be easily recognized, one for each alloy, following the order preliminary established above from the loss factor of cycle 30, which is now reproduced and stable for 200 superelastic cycles. The CAN sample has the highest damping capacity, with an average loss factor of $\eta = 0.20 \pm 0.01$. This result agrees with the previous works that motivated the present study [67,83,89]. The CAB, CANB and CANG samples follow in descending order, with a loss factor of $\eta = 0.100 \pm 0.006$, $\eta = 0.072 \pm 0.004$ and $\eta = 0.042 \pm 0.002$, respectively. The preliminary analysis that was carried out at the beginning, using the loss factor data from the individual micropillars of each sample, using the superelastic cycle number 30, is consistent with the final average behavior observed along the 200 cycles evaluated from the three pillars of each alloy. Together, these four alloys form a wide loss factor band, where the upper edge is delimited by the already documented ultrahigh damping capacity of the Cu–Al–Ni alloy [67], and the lower edge, with a value of only 20% of Cu–Al–Ni and without reported precedents, is delimited by the Cu–Al–Ni–Ga alloy.

However, before establishing any conclusion, we have to analyze some critical aspects influencing the experimental measure of damping by nano-compression tests. The first critical aspect is associated with the evolution on cycling of the nano-compression superelastic cycle shape, which evolves due to a training effect

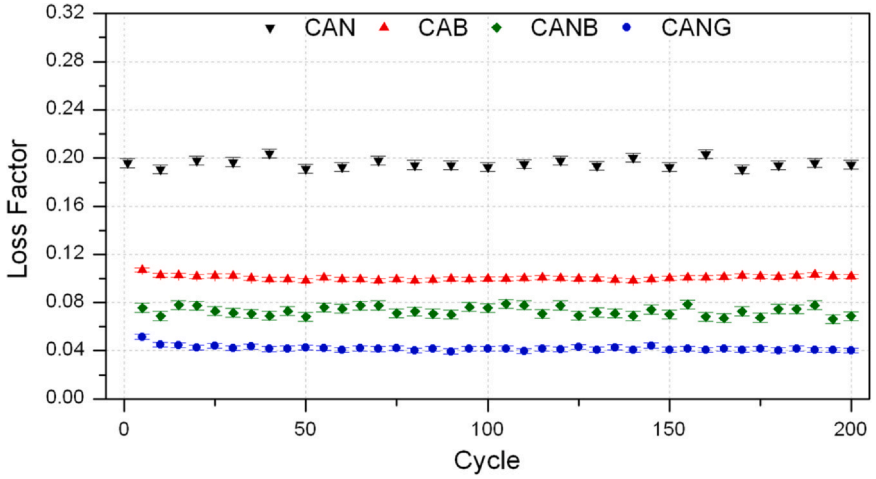

Fig. 6. Average loss factor as a function of cycling for each studied alloy. The results were averaged from the three micropillars studied in each alloy: CAN (downward black triangles), CAB (upward red triangles), CANB (green diamonds), and CANG (blue dots).

linked to the nucleation of the martensite plates. Indeed, the shape of the superelastic cycle evolves rather fast during the first cycles and more slowly between the cycles 10–50, being practically stabilized for the cycle 100 and beyond. This training effect was already reported in the literature [82,83,91], being confirmed in the present work, and this is the reason why the loss factor measured for the cycle 30 was the one used in Figs. 2 and 3, and cycle 50 was taken as reference in Fig. 4.

The second critical aspect concerns the reproducibility of the nano-compression cycles from one pillar to another because each micro/nano pillar exhibits a specific individuality, such as was recently discussed [83]. This individual behavior is more noticeable for tiny pillars, which are more affected by the particular milling conditions. As the objective of the present work is to comparatively study the damping behavior of different alloys at small scale, we intentionally avoided working on very small pillars, using pillars around 1 µm diameter for the comparison presented in Figs. 4 to 6. Obviously, the individual behavior of the pillars can be averaged with a good statistic approach, such as was tested in previous works [80,83], for arrays of 25 and 16 pillars respectively. For pillars in the range of 1 µm diameter, milled in similar conditions, the results, presented in Figs. 4 and 5, evidence a excellent reproducibility in both, cycle shape and loss factor, and three pillars are well enough to do the average plotted in Fig. 6.

The third critical aspect concerns the strain amplitude at which the loss factor is measured. Strictly speaking, in the case of non-linear mechanisms, as the superelastic behavior, the loss factor should be measured at constant strain amplitude, but this is a tricky task from an experimental point of view. Indeed, to work at constant strain amplitude, the displacement control mode must be used, but the superelastic plateau constitutes a so abrupt and fast displacement, up to 4% strain in 1 ms [67], that prevent the use of this control mode; the nanoindenter does not work properly, introducing experimental artifacts that modify even the shape of the cycle. Then, if the constant strain amplitude cannot be used, the alternative is to work at constant stress amplitude, through the load control mode, allowing fix the maximum load reached during the cycle. However, the maximum load necessarily change for pillars of different diameters and alloys, and here we have to remember that the conversion of load-displacement curves to stress-strain curves must be done a posteriori, such as was discussed in a previous work [80]. The nano-compression tests undergo a noticeable variation of the maximum stress when measuring in different pillars and alloys, as shown in Figs. 2 and 3, which in practice is difficult to avoid, even if the required maximum load is previously estimated. Although this effect represents an unavoidable experimental limitation, its influence can be qualitatively evaluated and the dependence of the loss factor on the stress amplitude was approached applying different maximum loads to the same pillar and measuring the variation of the loss factor. Fig. 7 shows a series of nano-compression tests between 190 and 580 MPa, so a ratio of three, applied on the same pillar shown in Fig. 2(a). The exhaustion of the first stage plateau occurs in all cases at the same stress and a further increase of the stress activates the secondary stage of the SIMT, whose unload proceed initially by an elastic recovery. Consequently, the increase of the maximum load in the elastic region produces only a slightly higher damping and, according to Eq. (1), the loss factor decreases. However, the recovery path of the SIMT strain can undergo some variations, introducing additional unexpected fluctuations of the loss factor. This description can be followed in Fig. 7, which allows evaluate the influence of stress amplitude on damping in about 25% for this rather high amplitude change. Consequently, it can be concluded that the differences observed for different alloys, which are presented in Fig. 6, cannot be attributed to the differences in amplitude and definitely we can conclude that they are associated with the intrinsic behavior of the alloy.

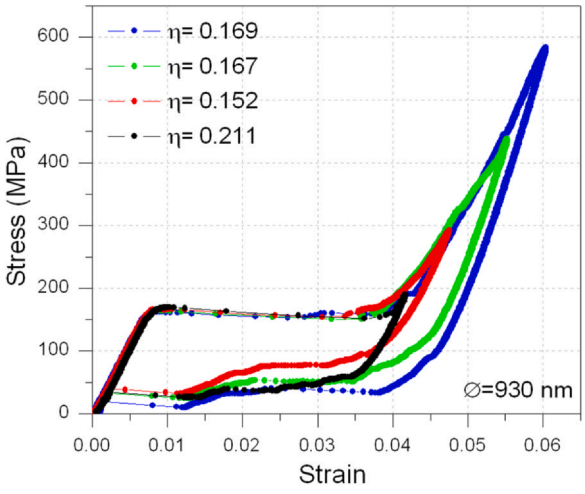

Fig. 7. Superelastic behavior measured in the pillar of Cu–Al–Ni alloy shown in Fig. 2(a), for four different maximum stress amplitude, and the loss factor of each cycle calculated from Eq. (1).

3.3. Size effect on damping at nanoscale

When establishing the experimental conditions for the present study, micropillars around 1 µm in diameter were intentionally used to obtain a good reproducibility, avoiding size effects. Indeed, a clear size effect on the critical stress for superelasticity was recently observed in Cu–Al–Ni [80] and Cu–Al–Be [81] SMA, which was attributed to the paucity of nucleation points (dislocations) for martensite in small confined volumes, requiring a higher stress for the homogeneous nucleation of martensite. So, before closing the discussion we can ask: Is there a size effect on damping?

The answer is yes, because small pillars of Cu–Al–Ni exhibit higher damping capacity than the macroscopic sample of these alloys [67], although no clear trend was found in the same alloy at nanoscale [80]. The difficulty to determine this potential dependence is coming from the aspects discussed in the previous section: individuality of the pillar behavior, size dependence of the critical stress for SIMT and stress amplitude variation during the tests. Then, in an attempt to answer the above question, a new series of pillars was milled in the quaternary alloy CANG, covering pillars from 2000 down to 250 nm in diameter, and trying to maintain the maximum stress amplitude in a small range of variation, which finally was between 600 and 900 MPa, so a ratio of only 1.5, for all the pillars. In Fig. 8, three examples of pillar images Fig. 8(a), (b), (c), in the small diameter range are shown, together with the nano-compression superelastic cycles, Fig. 8(d), (e), (f); the diameter of each pillar and the calculated loss factor are indicated in the figures. The increase of the loss factor when decreasing the diameter is evident in these plots, and the dependence of the damping coefficient on size can be clearly seen in the Fig. 9 where the values of the loss factor calculated for all the pillar series are presented. Indeed, whereas there is no evolution of the loss factor above 900 nm, for small pillars an increasing trend can be observed, which becomes exacerbated for very small pillars below 400 nm in diameter. Then we can conclude, from the present experiments, that there is a size effect on superelastic damping at the nanoscale.

The explanation is associated with the increase of the critical stress, which moves up the superelastic plateau when decreasing the pillar diameter. In addition, in small features and pillars, martensite plates span across the whole diameter of the pillar [83,90] and release the stored elastic energy, accumulated at the growing front [70], at the surface of the pillar. This elastic energy, stored during the forward MT, constitutes the driving force for the reverse MT. Hence,

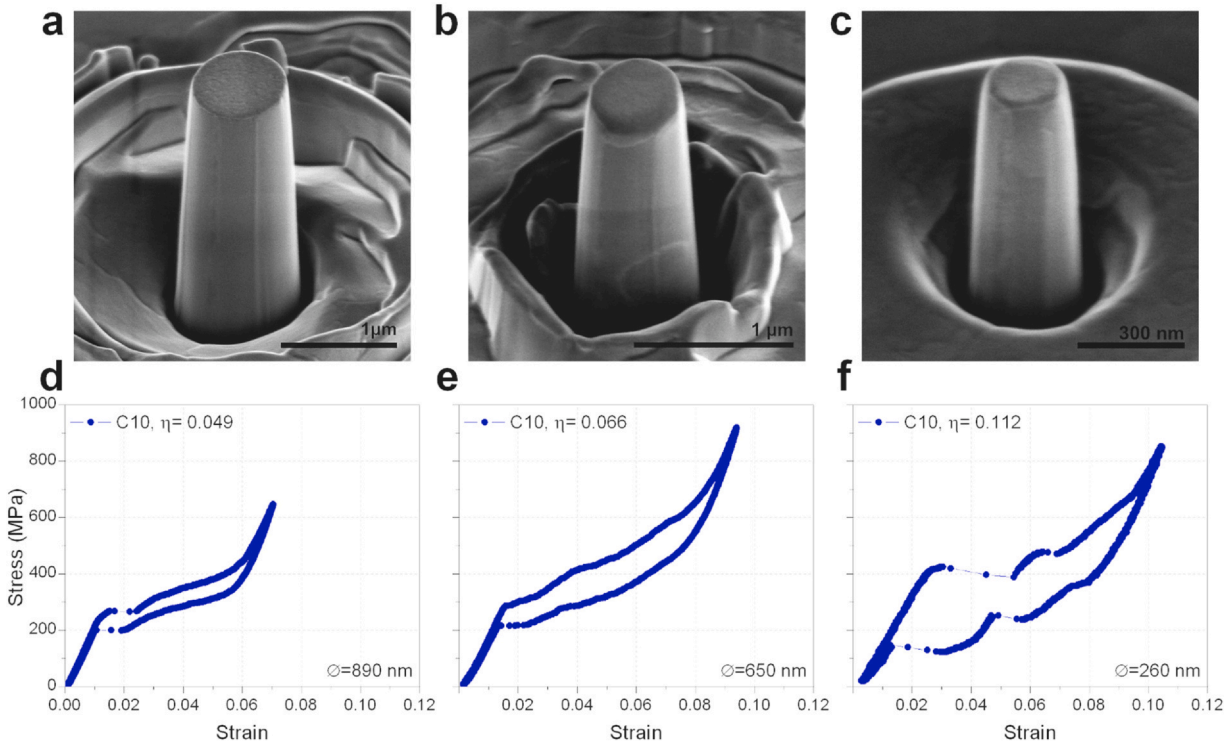

Fig. 8. Scanning electron microscopy images of three [001] oriented pillars milled on the sample of Cu–Al–Ni–Ga, with different diameters: (a) 890 nm, (b) 650 nm and (c) 260 nm. Plots of the stress-strain superelastic curves, obtained during the 10th nano-compression cycle on the above pillars, (d), (e), (f) respectively; the loss factor calculated from Eq. (1) is indicated.

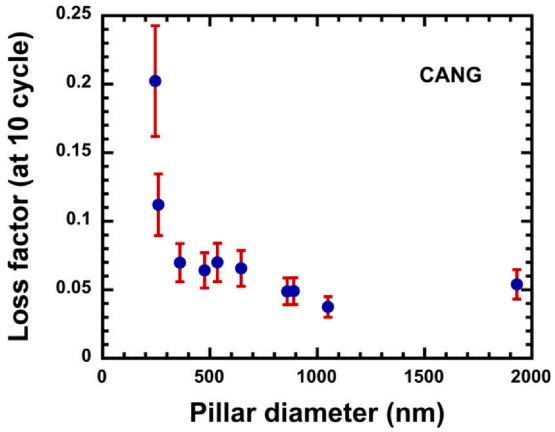

Fig. 9. Dependence of the loss factor, calculated from nano-compression tests, on the diameter of the pillar, observed in the Cu–Al–Ni–Ga alloy, which evidences the size effect on damping.

the release of the elastic energy delay the reverse transformation, such as it was experimentally verified by adiabatic calorimetry [92,93] and neutron diffraction [94], and during a superelastic test the reverse MT will take place at lower stresses. As a consequence of the increase of the stress for the forward MT and the decrease of the stress for the reverse one, there is a noticeable increase of the mechanical hysteresis and obviously of the loss factor. However, although this qualitative explanation allows justifying the observed results of damping at micro/nanoscale, the quantitative functional dependence of this size effect on damping is not yet found, remaining still an open question, and deeper studies are in progress to elucidate this aspect.

4. Conclusions

The experimental results obtained in this work allow a comparative analysis of the mechanical damping capacity, measured at the nanometer scale, in the following four Cu-based shape memory alloys: Cu–Al–Ni, Cu–Al–Be, Cu–Al–Ni–Be and Cu–Al–Ni–Ga. At the light of the presented results, the following conclusions can be drawn:

- Three [001] oriented single-crystal micropillars of comparable dimensions (about 1 μm in diameter) were studied for each alloy by nano-compression testing, which reveals as a well-adapted technique to measure damping at the nanoscale.
- All micropillars exhibited a fully closed superelastic behavior during 200 nano-compression cycles. The loss factor η was calculated for each superelastic cycle through the load-displacement curve to have a dimensionless and comparable damping index.
- Superelastic and damping behavior reproducibility was remarkable for each micropillar, and even between micropillars of the same alloy. This reproducibility was evidenced by the standard deviation when the loss factor values of the three micro-pillars of each alloy were averaged.
- In decreasing order, the average loss factor η for each alloy was: $\eta = 0.20 \pm 0.01$ for Cu–Al–Ni, $\eta = 0.100 \pm 0.006$ for Cu–Al–Be, $\eta = 0.072 \pm 0.004$ for Cu–Al–Ni–Be and $\eta = 0.042 \pm 0.002$ for Cu–Al–Ni–Ga. These four alloys offer a wide loss factor band for damping applications at the micro/nanoscale.

- A size effect of the superelastic loss factor on the diameter of the pillar was observed for the Cu–Al–Ni–Ga alloy, which is particularly noticeable below 400 nm. The origin of this size effect as well as the observed trend, are discussed in terms of the microscopic aspects of nucleation and growth of the martensite at small scale.

The above findings contribute to the fundamental understanding of the stress-induced martensitic transformation in confined volumes of micrometric order. These results also constitute a reference for engineering, since this type of micro/nano structures can potentially be integrated not only as sensors and actuators, but also as dampers in the design of MEMS or small hybrid material systems in order to improve their reliability.

Declaration of Competing Interest

The authors declare that they have no known competing financial interests or personal relationships that could have appeared to influence the work reported in this paper.

Acknowledgments

This research was supported by the Spanish Ministry of Economy and Competitiveness, MINECO, projects MAT2017-84069P and CONSOLIDER-INGENIO 2010 CSD2009-00013, as well as by the ELKARTEK-CEMAP project from the Industry Department of the Basque Government, and GIU-17/071 from the University of the Basque Country UPV/EHU, Spain. This work made use of the FIB and ICP facilities of the SGIKER from the UPV/EHU. The author V.F. acknowledges the Post-Doctoral Mobility Grant from the CONICET of Argentina, and J.F.G.-C. also acknowledges the Post-Doctoral Grant (ESPDOC18/37) from the UPV/EHU.

References

[1] E.I. Rivin, Handbook on Stiffness & Damping in Mechanical Design, ASME, New York, USA, 2010.
[2] A. Lago, D. Trabucco, A. Wood, Damping Technologies for Tall Buildings: Theory, Design, Guidance and Case Studies, Butterworth-Heinemann, Oxford, UK, 2019.
[3] A.M. Baz, Active and Passive Vibration Damping, John Wiley & Sons, Hoboken, NJ, USA, 2019.
[4] R. De Batist, Internal Friction of Structural Defects in Crystalline Solids, North-Holland Publishing Company, Amsterdam, Holland, 1972.
[5] A.S. Nowick, B.S. Berry, Anelastic Relaxation in Crystalline Solids, Academic Press, New York, USA, 1972.
[6] R.S. Lakes, Viscoelastic Solids, CRC Press, Boca Raton, USA, 1999.
[7] G. Fantozzi, Phenomenology and definitions, Mater. Sci. Forum 366–368 (2001) 3–31.
[8] J. San Juan, Mechanical spectroscopy, Mater. Sci. Forum 366–368 (2001) 32–73.
[9] M.S. Blanter, I.S. Golovin, H. Neuhäuser, H.R. Shinning, Internal Friction in Metallic Materials, Springer-Verlag, Berlin, Germany, 2007.
[10] R. De Batist, High damping materials - mechanisms and applications, J. Phys. Paris 44 (C9) (1983) 39–50.
[11] R. Schaller, High damping materials, Mater. Sci. Forum 366–368 (2001) 621–631.
[12] N. Igata, K. Nishiyama, K. Ota, Y. Yin, W. Wuttig, I.S. Golovin, J. Van Humbeeck, J. San Juan, Panel discussion on the applications of HDM, J. Alloys Compd. 355 (2003) 230–240.
[13] J. Van Humbeeck, J. Stoiber, L. Delaey, R. Gottard, The high damping capacity of shape memory alloys, Z. für Metallkd. 86 (1995) 176–183.
[14] R.B. Pérez-Sáez, V. Recarte, M.L. Nó, J. San Juan, Anelastic contribution and transformed volume fraction during martensitic transformation, Phys. Rev. B 54 (1998) 5684–5692.
[15] J. Van Humbeeck, Damping capacity of thermo-elastic martensite in shape memory alloys, J. Alloys Compd. 355 (2003) 58–64.
[16] J. San Juan, M.L. Nó, Damping behavior during martensitic transformation in shape memory alloys, J. Alloys Compd. 355 (2003) 65–71.
[17] T.W. Duerig, K.N. Melton, D. Stöckel, C.M. Wayman, Engineering Aspects of Shape Memory Alloys, Butterworth-Heinemann, London, UK, 1990.
[18] K. Otsuka, C.M. Wayman, Shape Memory Materials, Cambridge University Press, Cambridge, UK, 1998.
[19] K. Yamauchi, I. Ohkata, K. Tsuchiya, S. Miyazaki, Shape Memory and Superelastic Alloys: Technologies and Applications, Woodhead Publ. LTD, Cambridge, UK, 2011.
[20] R. Desroches, B. Smith, Shape memory alloys in seismic resistant design and retrofit: a critical review of their potential and limitations, J. Earthq. Eng. 7 (2004) 415–429.
[21] J. Van Humbeeck, S. Kustov, Active and passive damping of noise and vibrations through shape memory alloys: applications and mechanisms, Smart Mater. Struct. 14 (2005) S171–S185.
[22] L. Janke, C. Czaderski, M. Motavalli, J. Ruth, Applications of shape memory alloys in civil engineering structures - overview, limits and new ideas, Mater. Struct. 38 (2005) 578–592.
[23] G. Song, N. Ma, H.N. Li, Applications of shape memory alloys in civil structures, Eng. Struct. 28 (2006) 1266–1274.
[24] K. Otsuka, X. Ren, Physical metallurgy of Ti–Ni-based shape memory alloys, Prog. Mater. Sci. 50 (2005) 511–678.
[25] J.M. Jani, M. Leary, A. Subic, M.A. Gibson, A review of shape memory alloy research, applications and opportunities, Mater. Des. 56 (2014) 1078–1113.
[26] K. Otsuka, K. Shimizu, Memory effect and thermoelastic martensitic transformation in Cu–Al–Ni alloy, Scr. Metall. 4 (1970) 469–472.
[27] K. Otsuka, C.M. Wayman, K. Nakai, H. Sakamoto, K. Shimizu, Superelasticity effects and stress-induced martensitic transformations in Cu–Al–Ni alloys, Acta Met. 24 (1976) 207–226.
[28] K. Otsuka, H. Sakamoto, K. Shimizu, Successive stress-induced martensitic transformations and associated transformation pseudoelasticity in Cu–Al–Ni alloys, Acta Met. 27 (1979) 585–601.
[29] T. Saburi, C.M. Wayman, K. Takata, S. Nenno, The shape memory mechanism in 18R martensitic alloys, Acta Met. 28 (1980) 15–32.
[30] H. Horikawa, S. Ichinose, K. Morii, S. Miyazaki, K. Otsuka, Orientation dependence of $\beta \Rightarrow \beta'_1$ stress-induced martensitic transformation in a Cu–Al–Ni alloy, Metall. Trans. A 19A (1988) 915-823.
[31] Ll Mañosa, M. Jurado, A. Planes, J. Zarestky, T. Lograsso, C. Stassi, Elastic constants of bcc Cu–Al–Ni alloys, Phys. Rev. B 49 (1994) 9969–9972.
[32] V. Novák, P. Sittner, D. Vokoun, N. Zárubová, On the anisotropy of martensitic transformations in Cu-based alloys, Mat. Sci. Eng. A 273–275 (1999) 280–285.
[33] V. Recarte, J.I. Pérez-Landazabal, M.L. Nó, J. San Juan, Study by resonant ultrasound spectroscopy of the elastic constants of the β phase in Cu–Al–Ni shape memory alloys, Mater. Sci. Eng. A 370 (2004) 488–491.
[34] H. Sakamoto, Y. Nakai, K. Shimizu, Optimization of composition for the appearance of Pseudoelasticity due to consecutive transformations in Cu–Al–Ni alloy single crystals, Trans. JIM 28 (10) (1987) 765–772.
[35] V. Recarte, R.B. Pérez-Sáez, J. San Juan, E.H. Bocanegra, M.L. Nó, Influence of Al and Ni concentration on the martensitic transformation in Cu–Al–Ni shape memory alloys, Metall. Mater. Trans. A 33 (2002) 2581–2591.
[36] J. Van Humbeeck, M. Chandrasekaran, L. Delay, Influence of post quench ageing in the beta-phase on the transformation characteristics and the physical and mechanical properties of martensite in a Cu–Al–Ni shape memory alloy, ISIJ Int. 29 (1989) 388–394.
[37] H. Sakamoto, K. Shimizu, Effect of heat treatments on thermally formed martensite phases in monocrystalline Cu–Al–Ni shape memory alloy, ISIJ Int. 29 (1989) 395–404.
[38] V. Recarte, I. Hurtado, J. Herreros, M.L. Nó, J. San Juan, Precipitation of the stable phases in Cu–Al–Ni shape memory alloys, Scr. Mater. 34 (1996) 255–260.
[39] V. Recarte, R.B. Pérez-Sáez, M.L. Nó, J. San Juan, Evolution of martensitic transformation in Cu–Al–Ni shape memory alloys during low-temperature aging, J. Mat. Res. 14 (1999) 2806–2813.
[40] N. Suresh, U. Ramamurty, Aging response and its effect on the functional properties of Cu–Al–Ni shape memory alloys, J. Alloys Compd. 449 (2008) 113–118.
[41] V. Novák, J. Malimánek, N. Zárubová, Martensitic transformations in single crystals of Cu–Al–Ni induced by tensile stress, Mater. Sci. Eng. A 191 (1995) 193–201.
[42] R. Gastien, C.E. Corbellani, M. Sade, F.C. Lovey, Thermal and pseudoelastic cycling in Cu–14.1Al–4.2Ni (wt%) single crystals, Acta Mater. 53 (2005) 1685–1691.
[43] C. Picornell, J. Pons, E. Cesari, Mechanical stabilisation and anomalous behaviour of the stress-strain loops in Cu–Al–Ni single crystals, Scr. Mater. 54 (2006) 459–463.
[44] A. Ibarra, J. San Juan, E.H. Bocanegra, D. Caillard, M.L. Nó, "In situ" and "Post-morten" TEM study of the super-elastic effect in Cu-Al-Ni shape memory alloys, Mater. Sci. Eng. A 438–440 (2006) 787–790.
[45] A. Ibarra, J. San Juan, E.H. Bocanegra, M.L. Nó, Evolution of microstructure and thermomechanical properties during superelastic compression cycling in Cu–Al–Ni single crystals, Acta Mater. 55 (2007) 4789–4798.
[46] H. Fu, S. Xu, H. Zhao, H. Dong, J. Xie, Cyclic stress-strain response of directionally solidified polycrystalline Cu–Al–Ni shape memory alloys, J. Alloys Compd. 714 (2017) 154–159.
[47] I. López-Ferreño, J.F. Gómez-Cortés, T. Breczewski, I. Ruiz-Larrea, M.L. Nó, J.M. San Juan, High-temperature shape memory alloys based on the Cu-Al-Ni system: design and thermomechanical characterization, J. Mater. Res. Technol. 9 (2020) 9972–9984.
[48] S. Belkahla, H. Flores Zuñiga, G. Guenin, Elaboration and characterization of new low temperature shape memory Cu–Al–Be alloys, Mater. Sci. Eng. A 169 (1993) 119–124.
[49] E. Cingolani, R. Stalmans, J. Van Humbeeck, M. Ahlers, Influence of thermal treatments on the long range order and the two way shape memory effect induced by stabilization in Cu–Al–Be single crystals, Mater. Sci. Eng. A 268 (1999) 109–115.
[50] N. Siredey, A. Eberhardt, Fatigue behavior of Cu–Al–Be shape memory single crystals, Mater. Sci. Eng. A 290 (2000) 171–179.

[51] S. Kustov, M. Morin, E. Cesari, On the instantaneous stabilization in Cu–Al–Be β_1 martensite, Scr. Mater. 50 (2004) 219–224.
[52] M. Sade, A. Yawny, F.C. Lovey, V. Torra, Pseudoelasticity of Cu-Al-Be single crystals: unexpected mechanical behavior, Mater. Sci. Eng. A 528 (2011) 7871–7877.
[53] F. de Castro Bubani, M. Sade, V. Torra, F. Lovey, A. Yawny, Stress induced martensitic transformation and phases stability in Cu–Al–Be shape memory single cristals, Mater. Sci. Eng. A 583 (2013) 129–139.
[54] I. López-Ferreño, T. Breczewski, I. Ruiz-Larrea, M.L. Nó, J. San Juan, Thermal treatments and transformation behavior of Cu–Al–Be shape memory alloys, J. Alloys Compd. 577S (2013) S463–S467.
[55] I. López-Ferreño, T. Breczewski, G.A. López, M.L. Nó, J. San Juan, Stress-assisted atomic diffusion in metastable austenite $D0_3$ phase of Cu–Al–Be shape memory alloys, Scr. Mater. 124 (2016) 155–159.
[56] J.W. Gardner, V.K. Varadan, O.O. Awadelkarim, Microsensors MEMS and Smart Devices, John Wiley & Sons, Chichester, UK, 2001.
[57] M. Kohl, Shape Memory Microactuators, Springer-Verlag, Berlin, Germany, 2004.
[58] S. Miyazaki, Y.Q. Fu, W.M. Huang, Thin Film Shape Memory Alloys, Cambridge University Press, Cambridge, UK, 2009.
[59] A.C. Fischer-Cripps, Nanoindentation, Springer, New York, USA, 2004.
[60] C.A. Schuh, Nanoindentation studies in materials, Mater. Today 9 (2006) 32–40.
[61] M.D. Uchic, D.M. Dimiduk, J.N. Florando, W.D. Nix, Sample dimensions influence strength and crystal plasticity, Science 305 (2004) 986–989.
[62] K. Gall, J. Diao, M.L. Dunn, The strength of gold nanowires, Nano Lett. 4 (2004) 2431–2436.
[63] J.R. Greer, W.C. Oliver, W.D. Nix, Size dependence of mechanical properties of gold at the micron scale in the absence of strain gradients, Acta Mater. 53 (2005) 1821–1830.
[64] C.P. Frick, S. Orso, E. Arzt, Loss of pseudoelasticity in nickel-titanium sub-micron compression pillars, Acta Mater. 131 (2007) 3845–3855.
[65] J. San Juan, M.L. Nó, C.A. Schuh, Superelasticity and shape memory in micro- and nanometer-scale pillars, Adv. Mater. 20 (2008) 272–278.
[66] J. San Juan, M.L. Nó, C.A. Schuh, Thermomechanical behavior at the nanoscale and size effects in shape memory alloys, J. Mater. Res. 26 (2011) 2461–2469.
[67] J. San Juan, M.L. Nó, C.A. Schuh, Nanoscale shape-memory alloys for ultrahigh mechanical damping, Nat. Nanotechnol. 4 (2009) 415–419.
[68] B.G. Clark, D.S. Gianola, O. Kraft, C.P. Frick, Size independent shape memory behavior of nickel-titanium, Adv. Eng. Mater. 12 (2010) 808–815.
[69] J.R. Greer, J.T.M. De Hosson, Plasticity in small-sized metallic systems: intrinsic versus extrinsic size effect, Prog. Mater. Sci. 56 (2011) 654–724.
[70] M.L. Nó, A. Ibarra, D. Caillard, J. San Juan, Quantitative analysis of stress-induced martensites by in situ transmission electron microscopy superelastic tests in Cu–Al–Ni shape memory alloys, Acta Mater. 58 (2010) 6181–6193.
[71] J. San Juan, M.L. Nó, Superelasticity and shape memory at nanoscale: size effects on the martensitic transformation, J. Alloys Compd. 577S (2013) S25–S29.
[72] N. Ozdemir, I. Karaman, N.A. Mara, Y.I. Chumlyakov, H.E. Karaca, Size effects in the superelastic response of Ni54Fe19Ga27 shape memory alloy pillars with a two stage martensitic transformation, Acta Mater. 60 (2012) 5670–5685.
[73] A. Lai, Z. Du, C.L. Gan, C.A. Schuh, Shape memory and superelastic ceramics at small scale, Science 341 (2013) 1505–1508.
[74] Z. Du, X.M. Zeng, A. Lai, S. Amini, A. Miserez, C.A. Schuh, C.L. Gan, Size effects and shape memory properties in ZrO_2 ceramic micro- and nano-pillars, Scr. Mater. 101 (2015) 40–43.
[75] J. Fornell, N. Tuncer, C.A. Schuh, Orientation dependence in superelastic Cu–Al–Mn–Ni micropillars, J. Alloys Compd. 693 (2017) 1205–1213.
[76] F. Xiao, K.J. Chu, X.J. Jin, F.Z. Ren, T. Fukuda, T. Kakeshita, Q.P. Sun, Size effect on the mechanical behavior of single crystalline Fe-31.2Pd (at%) micropillars, Scr. Mater. 152 (2018) 141–145.
[77] M. Vronka, M. Karlik, J. Vesely, J. Manak, O. Heczko, Suppresion of twinning mechanism on nanoscale: size effect in Cu–Ni–Al shape memory alloy, J. Mater. Sci. 54 (2019) 6586–6593.
[78] F. Xiao, K.J. Chu, F.Z. Ren, Superelasticity of micropillar of single crystalline Fe_3Pt, Materialia 9 (2020) 100534.
[79] P. Hua, K. Chu, F. Ren, Q. Sun, Cyclic phase transformation of nanocrystalline NiTi at microscale, Acta Mater. 185 (2020) 507–517.
[80] J.F. Gómez-Cortés, M.L. Nó, I. López-Ferreño, J. Hernandez-Saz, S.I. Molina, A. Chuvilin, J.M. San Juan, Size effect and scaling power law for superelasticity in shape memory alloy at the nanoscale, Nat. Nanotechnol. 12 (2017) 790–797.
[81] V. Fuster, J.F. Gómez-Cortés, M.L. Nó, J.M. San Juan, Universal scaling law for the size effect on superelasticity at the nanoscale promotes the use of shape-memory alloys in stretchable devices, Adv. Electron. Mater. 6 (2020) 1900741.
[82] J. San Juan, J.F. Gómez-Cortés, G.A. López, C. Jiao, M.L. Nó, Long-term superelastic cycling at nanoscale in Cu–Al–Ni shape memory alloy micropillars, Appl. Phys. Lett. 104 (2014) 011901.
[83] J.F. Gómez-Cortés, M.L. Nó, I. Ruíz-Larrea, T. Breczewski, A. López-Echarri, C.A. Schuh, J.M. San Juan, Ultrahigh superelastic damping at the nanoscale: a robust phenomenon to improve smart MEMS devices, Acta Mater. 166 (2019) 346–356.
[84] Y.T. Cheng, Vacuum packaging technology, J. MEMS 11 (2002) 556–565.
[85] V. Kaajaraki, Practical MEMS, Small Gear Publishing, USA, 2009.
[86] A.D. Roming, M.T. Dugger, P.J. McWhorter, Materials issues in micro electro mechanical devices: science, engineering, manufacturing and reliability, Acta Mater. 51 (2003) 5837–5866.
[87] P. Lorenzo, Aleaciones con Memoria de Forma (SMA) para condiciones extremas: Muy bajas temperaturas, PhD Thesis (in Spanish), University of the Basque Country, Bilbao, Spain, 2021.
[88] H. Zhang, B.E. Chuster, Q. Wei, K.T. Ramesh, The design of accurate micro-compression experiments, Scr. Mater. 54 (2006) 181–186.
[89] J.F. Gómez-Cortés, M.L. Nó, A. López-Echarri, I. Ruíz-Larrea, T. Breczewski, J.M. San Juan, Anomalous behavior during nano-compression superelastic tests on Cu–Al–Ni shape memory alloy micropillars, Phys. Status Solidi A 215 (2018) 1800340.
[90] S.M. Ueland, C.A. Schuh, Transition from many domain to single domain martensite morfology in small-scale shape memory alloys, Acta Mater. 61 (2013) 5618–5625.
[91] J. San Juan, M.L. Nó, C.A. Schuh, Superelastic cycling of Cu–Al–Ni shape memory alloy micropillars, Acta Mater. 60 (2012) 4093–4106.
[92] J. Rodriguez-Aseguinolaza, I. Ruiz-Larrea, M.L. Nó, A. López Echarri, J.M. San Juan, Temperature memory effect in Cu–Al–Ni shape memory alloys studied by adiabatic calorimetry, Acta Mater. 56 (2008) 3711–3722.
[93] J. Rodriguez-Aseguinolaza, I. Ruiz-Larrea, M.L. Nó, A. López Echarri, J. San Juan, A new quantitative approach to the thermoelastic martensitic transformation: the density of elastic states, Acta Mater. 56 (2008) 6283–6290.
[94] I. Ruiz-Larrea, A. López-Echarri, J.F. Gómez-Cortés, M.L. Nó, D.W. Brown, L. Balogh, T. Breczewski, J. San Juan, Strain relaxation in Cu–Al–Ni shape memory alloys studied by in situ neutron diffraction experiments, J. Appl. Phys. 125 (2019) 082536.